IOP Publishing Journal of Physics B: Atomic, Molecular and Optical Physics
J. Phys. B: At. Mol. Opt. Phys. **50** (2017) 034002 (8pp) doi:10.1088/1361-6455/50/3/034002

# Born in weak fields: below-threshold photoelectron dynamics

**J B Williams[1,5], U Saalmann[2], F Trinter[3], M S Schöffler[3], M Weller[3], P Burzynski[3], C Goihl[3], K Henrichs[3], C Janke[3], B Griffin[1], G Kastirke[3], J Neff[3], M Pitzer[3], M Waitz[3], Y Yang[3], G Schiwietz[4], S Zeller[3], T Jahnke[3] and R Dörner[3]**

[1] Department of Physics, University of Nevada, Reno, NV 89557, USA
[2] Max Planck Institute for the Physics of Complex Systems, Nöthnitzer Str. 38, D-01187 Dresden, Germany
[3] Institut für Kernphysik, J W Goethe Universität, Max-von-Laue-Str. 1, D-60438 Frankfurt, Germany
[4] Helmholtz-Zentrum Berlin für Materialien und Energie, Institute G-ISRR, Hahn-Meitner-Platz 1, D-14109 Berlin, Germany

E-mail: jbwilliams@unr.edu

Received 8 August 2016, revised 15 September 2016
Accepted for publication 21 September 2016
Published 13 January 2017

**Abstract**

We investigate the dynamics of ultra-low kinetic energy photoelectrons. Many experimental techniques employed for the detection of photoelectrons require the presence of (more or less) weak electric extraction fields in order to perform the measurement. Our studies show that ultra-low energy photoelectrons exhibit a characteristic shift in their apparent measured momentum when the target system is exposed to such static electric fields. Already fields as weak as 1 V cm$^{-1}$ have an observable influence on the detected electron momentum. This apparent shift is demonstrated by an experiment on zero energy photoelectrons emitted from He and explained through theoretical model calculations.

Keywords: COLTRIMS, photo-ionization, below-threshold photo-ionization, Rydberg

(Some figures may appear in colour only in the online journal)

## 1. Introduction

The Stark effect caused by *strong* electric fields significantly modifies photoionization. It shifts thresholds and induces additional resonances [1–3]. For highly excited states however, already very weak fields, i.e. $F = 1 \ldots 40$ V cm$^{-1}$ and higher, lead to complex electron dynamics below threshold in the time domain [4] as such static electric fields can asymmetrically tilt the atomic potential and allow electrons to escape over this tilted barrier. Such Rydberg dynamics have been studied for many years, e.g. by employing zero electron kinetic energy (ZEKE) spectroscopy [5, 6]. While in the cases mentioned so far, the effect of the static electric field on atoms was under investigation, it turns out that a variety of effects may occur already due to electric fields employed in many measurement techniques as a part of the experimental apparatus as well. A very intriguing example can be found with the occurrence of interference fringes in the photoelectron momenta in experiments employing velocity map imaging spectroscopy [7]. Furthermore, in the realm of strong field ionization, a so called 'low-energy structure' was observed in many experiments [8, 9]. Most recently, this feature has been investigated in more detail [10–16] and finally even lower energy electrons have been found to be caused by the ionization of highly excited states by the weak electric extraction field of the measurement setup [17].

Here we perform an extensive study of the effect of weak extraction fields on the measurement employing synchrotron radiation to create photoelectrons from helium atoms close to the ionization threshold in a controlled way.

[5] This article belongs to the Special Issue: Emerging Leaders, which features invited work from the best early-career researchers working within the scope of *J. Phys.* B. This project is part of the *Journal of Physics* series' 50th anniversary celebrations in 2017. Joshua Williams was selected by the Editorial Board of *J. Phys.* B as an Emerging Leader.

 

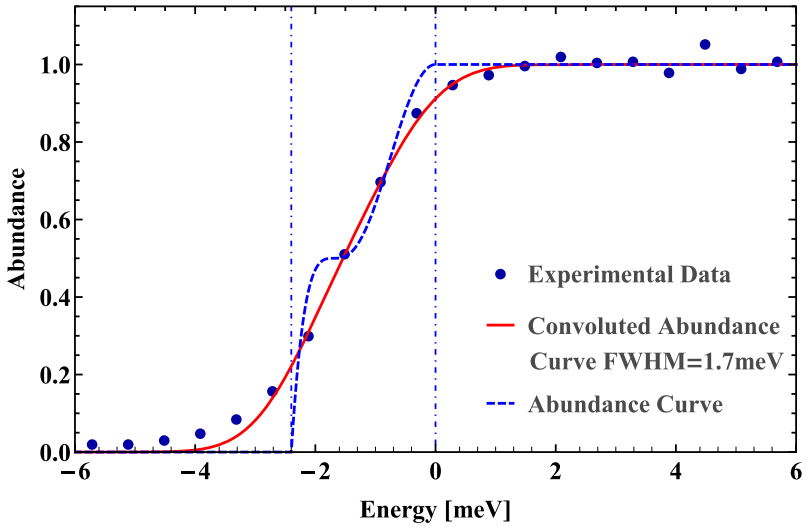


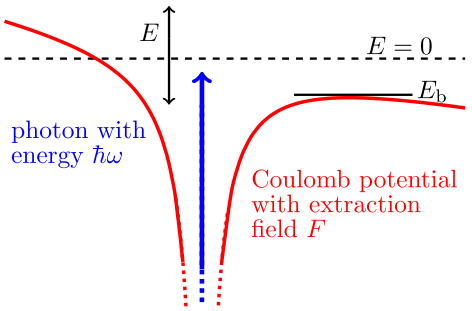


Sketch explaining the scenario and the definition of energy $E$. The initial binding energy $E_0$ is much lower and thus not visible here.

**Figure 1.** Experimental and theoretical electron abundance versus photon energy (which is the photon energy offset by the field-free threshold). Blue dashed curve is the theoretical abundance for a 10 V cm$^{-1}$ extraction field, solid red line is the theoretical abundance curve convoluted with the photon resolution of 1.7 meV, and blue dots are experimental data. The vertical blue lines denote the $E_b$ =−2.4 meV and the field-free threshold.

The photoelectron shows a negative apparent momentum for photon energies below the field-free threshold in the direction of the weak electric extraction field. This apparent momentum shift increases as the field strength is increased. The measured results are nicely reproducible by theoretical calculations. The sketch shown in figure 1 depicts the physical situation at the heart of the observed effect. In a fully classical picture, the following happens: the weak electrostatic field bends the atomic potential along the field direction, which is in the following denoted as the $z$-axis. As the other spatial directions are not effected by the electric field, the potential becomes asymmetric, yielding an ionization threshold which depends on the emission direction of the emerging photoelectron. While intuitively it seems that this directional shift of the ionization potential can be neglected for very weak electric fields, it has surprisingly large contributions on zero kinetic energy electrons as demonstrated in the following sections. The maximum shift of the ionization threshold, for example, for an electric field of only 10 V cm$^{-1}$ turns out to be as high as $E_b = -2.4$ meV.

## 2. Theoretical model

Investigations of the electron dynamics induced by strong long-wavelength (800 nm) laser pulses [17] have shown that the final momentum distribution in the region of small momenta is dominated by over-barrier dynamics with the barrier formed by the attractive Coulomb potential of the ion and homogeneous extraction field $F$, cf sketch in figure 1. It was verified that quantum effects do not play a role, which is due to the weakness of the field $F$, that renders any action very large. This allows us to study the threshold dynamics classically with the Stark Hamiltonian written in cylindrical coordinates $\{\rho, z\}$

$$H = \frac{1}{2}[p_\varrho{}^2 + p_z{}^2] - \frac{1}{r} - Fz \qquad \text{with} \quad r \equiv \sqrt{\varrho^2 + z^2}. \tag{1}$$

We can omit the azimuthal angle $\varphi$ since the independence of the initial state of $\varphi$ is preserved throughout.

The barrier formed by the two potential terms in (1) is located at $z_b = 1/\sqrt{F}$ with the top at $E_b = -2\sqrt{F}$. Typical values (for $F = 10$ V cm$^{-1}$) are $z_b \approx 1$ $\mu$m and $E_b \approx -2.4$ meV, as noted before. Since the distance is much larger than the initial extension of the two helium electrons one may launch an ensemble of trajectories from the Coulomb singularity and calculate their final momentum distribution.

To cope numerically with the Coulomb singularity it is advantageous to use squared parabolic (or semi-parabolic) coordinates $\{u, v\}$

$$u = \sqrt{r + z}, \quad p_u = \sqrt{r - z}\, p_\rho + \sqrt{r + z}\, p_z, \tag{2a}$$

$$v = \sqrt{r - z}, \quad p_v = \sqrt{r - z}\, p_\rho - \sqrt{r + z}\, p_z, \tag{2b}$$

for which we get two separated Hamiltonians [18]

$$H_u = \frac{1}{2}p_u^2 - Eu^2 - \frac{F}{2}u^4 - 1, \tag{3a}$$

$$H_v = \frac{1}{2}p_v^2 - Ev^2 + \frac{F}{2}v^4 - 1, \tag{3b}$$

with the (separation) condition $E_u + E_v = 0$. One should note that $E$, the energy of the electron, becomes in the transformation to the new coordinates a parameter in the Hamiltonians. Most importantly for the numerical calculations is the fact that the two Hamiltonians (3) come with a new time $\tau$ that is connected to the old time $t$ by $\mathrm{d}t = [u^2 + v^2]\mathrm{d}\tau$. Apparently $t$ is 'slowed down' when $u$ and $v$ are small, i.e. near the singularity at $u = v = 0$.

It remains to specify the initial conditions in terms of the new variables. Since trajectories are launched at the Coulomb

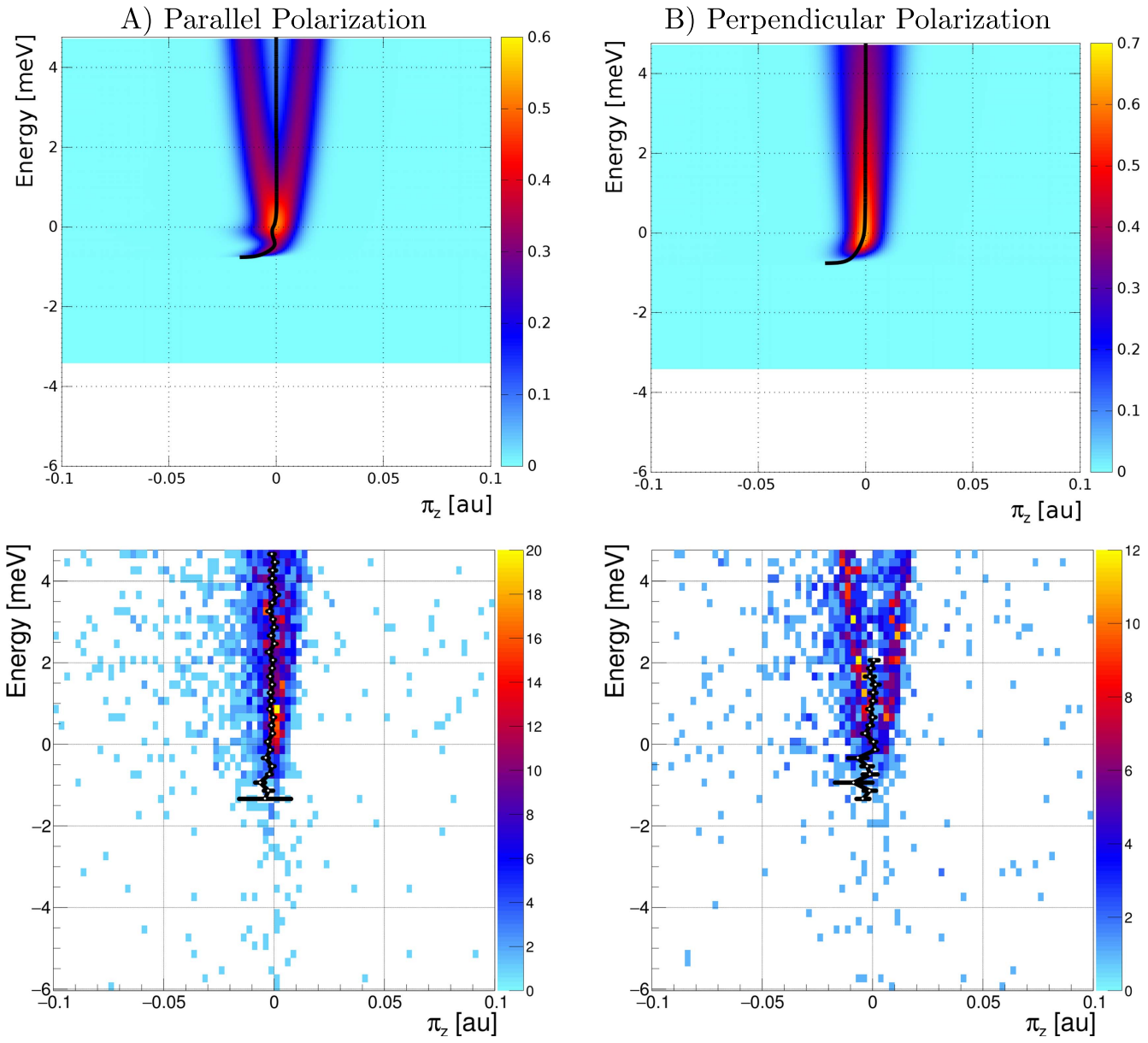


**Figure 2.** The energy (photon energy offset by to the field-free threshold) verse the effective electron momentum in the $z$-direction with the color scale indicating the counts for a 1 V cm$^{-1}$ extraction field. Top row shows theoretical calculations and the bottom row shows experimental data. The overlaid vertical black curve shows the mean value of the momentum distribution. On the bottom row, the horizontal black line is the fit error of the mean which result from the Gaussian fit. In column (A) the polarization is orientated parallel to the extraction field. In column (B) the polarization is orientated perpendicular to the extraction field.

singularity it is $u(\tau = 0) = v(\tau = 0) = 0$. Further a trajectory is characterized by the energy $E$ and the initial angle $\theta_i = \theta(t = 0)$, which is the angle of the initial momentum and the $z$-axis. It turns out that all conditions are fulfilled for $p_u(\tau = 0) = 2\cos(\theta_i/2)$ and $p_v(\tau = 0) = 2\sin(\theta_i/2)$. Note that $E_u = +\cos\theta_i$ and $E_v = -\cos\theta_i$, i.e. the launching direction reflects the partition of energy between the $u$ and $v$ degrees of freedom.

In order to calculate the measured momentum maps we have to choose a set of initial conditions with proper weights according to the excitation process by the linearly polarized single photon. We chose $P(E_i, \theta_i) = \bar{P}(E_i)\widetilde{P}(\theta_i)$ with

$$\bar{P}(E) = \frac{1}{\pi\sqrt{\Delta}}\exp(-[E - E_0 - \hbar\omega]^2/\Delta^2) \tag{4a}$$

$$\widetilde{P}(\theta) = \begin{cases} P_{\parallel}(\theta) = \frac{3}{2}\sin\theta\cos^2\theta \\ P_{\perp}(\theta) = \frac{3}{4}\sin^3\theta \end{cases} \tag{4b}$$

with $E_0$ the helium ground-state energy and $\hbar\omega$ the photon energy. The two situations 'parallel' and 'perpendicular' refer to the relation of the synchrotron polarization vector and the direction of the extraction field. The distributions in

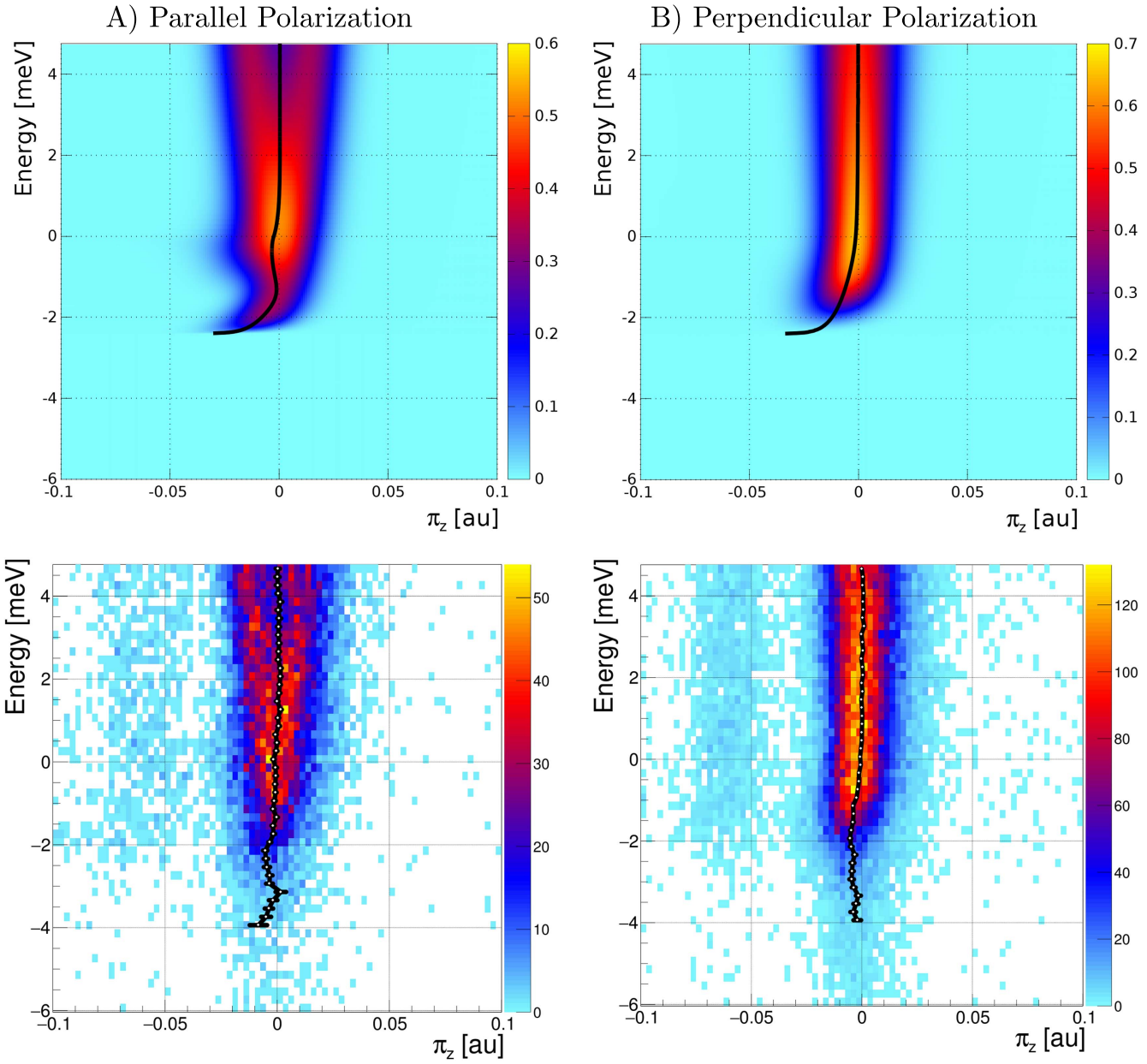


**Figure 3.** The energy (photon energy offset by to the field-free threshold) versus the effective electron momentum in the $z$-direction with the color scale indicating the counts for a 10 V cm$^{-1}$ extraction field. Top row shows theoretical calculations and the bottom row shows experimental data. The overlaid vertical black curve shows the mean value of the momentum distribution. On the bottom row, the horizontal black line is the fit error of the mean which result from the Gaussian fit. In column (A) the polarization is orientated parallel to the extraction field. In column (B) the polarization is orientated perpendicular to the extraction field.

equation (4) assume a single-photon excitation from an s-state, which separates into an an angular distribution $\widetilde{P}$ corresponding to a p-state and an energy distribution depending on the Fourier transform of the driving pulse. Assuming a Gaussian pulse yields a Gaussian peak $\bar{P}$ centered at $E_0 + \hbar\omega$ with a width of $\Delta$, which is given by the inverse pulse duration.

Note that for an energy $E$ above the barrier ($E_\mathrm{b} < E$) and below the field-free threshold ($E < 0$) only initial angles $\theta_\mathrm{i} < \theta_*$ with $\theta_* = \arccos(E^2/2F - 1)$ lead to free motion [17]. For example, for $E = E_\mathrm{b}$ it is $\theta_* = 0$, for $E = E_\mathrm{b}/2$ it is $\theta_* = 2\pi/3$, and for $E = 0$ it is $\theta^* = \pi$. Thus one can calculate the abundance as a function of the energy

$$S_\parallel(E) = \int_0^{\theta_*(E)} \mathrm{d}\theta\, P_\parallel(\theta) = \frac{1 - \cos^3\theta_*(E)}{2}, \qquad (5)$$

which results with $\cos\theta_*(E) = E^2/2F - 1$ in equation (8), which was used for calibrating the energy in the measured data, cf figure 1 above.

One can easily obtain the $\{\varrho, z\}$ coordinates by the inverse transformation of equation (2). Asymptotically, i.e. beyond the interaction region, the motion along the extraction

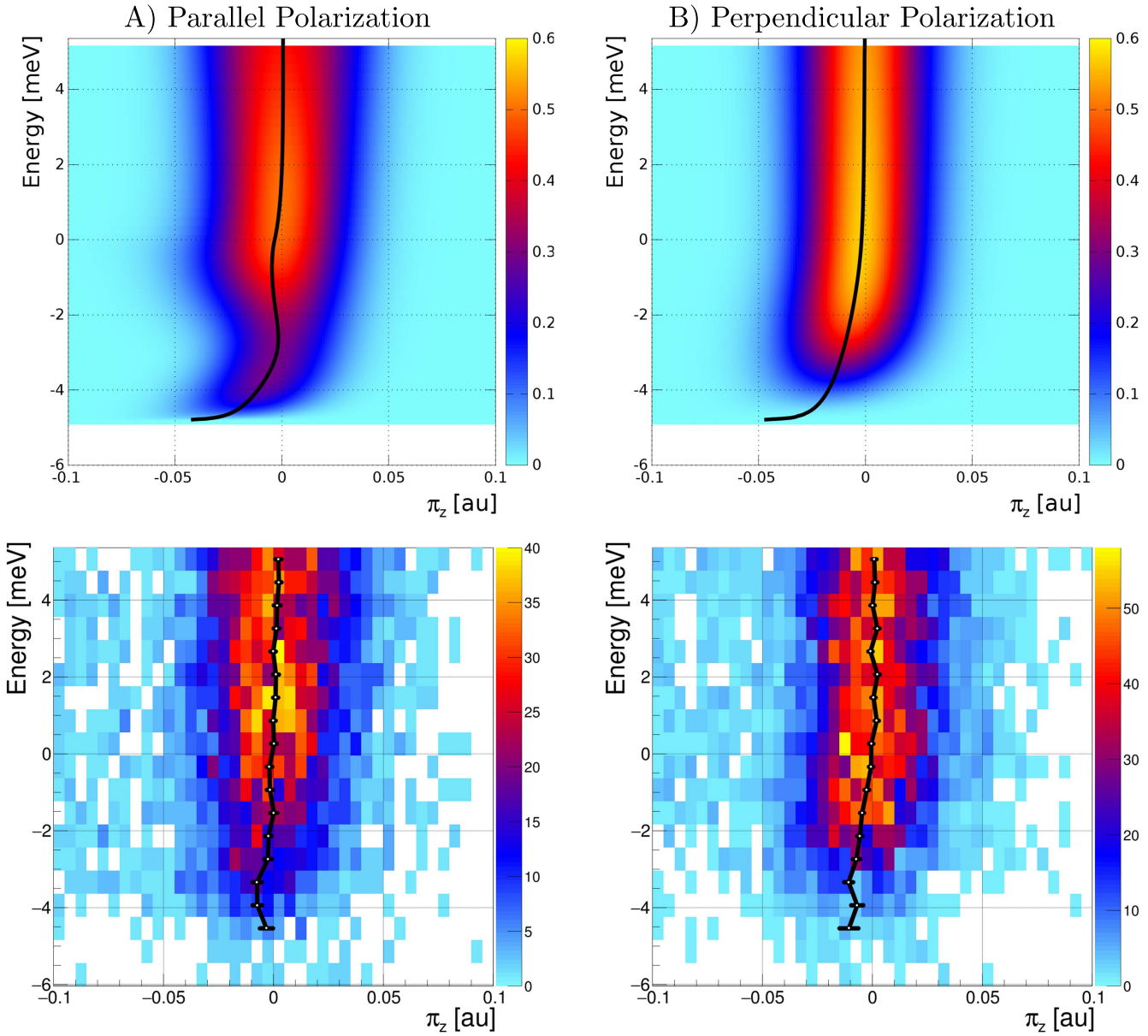


**Figure 4.** The energy (photon energy offset by to the field-free threshold) versus the effective electron momentum in the $z$-direction with the color scale indicating the counts for a 40 V cm$^{-1}$ extraction field. Top row shows theoretical calculations and the bottom row shows experimental data. The overlaid vertical black curve shows the mean value of the momentum distribution. On the bottom row, the horizontal black line is the fit error of the mean which result from the Gaussian fit. In column (A) the polarization is orientated parallel to the extraction field. In column (B) the polarization is orientated perpendicular to the extraction field.

field is

$$z(t) = z_0 + \pi_z t + \frac{F}{2}t^2 \quad \text{and} \quad p_z(t) = \pi_z + Ft, \tag{6}$$

from which one can deduce the effective momentum as

$$\pi_z = \frac{z(t_{\text{of}}) - z_0}{t_{\text{of}}} - \frac{F\ t_{\text{of}}}{2} \quad \text{or} \quad \pi_z = p_z(t_{\text{of}}) - F\ t_{\text{of}}. \tag{7}$$

Note that the rhs of both equations are independent of the time of flight $t_{\text{of}}$, provided $t_{\text{of}}$ is sufficiently large. Whereas the experimental data are obtained by the 1st equation, the theoretical approach uses the 2nd one.

## 3. Experimental setup and calibration procedure

In the present work we utilized Cold Target Recoil Ion Momentum Spectroscopy (COLTRIMS) [19–21] to measure low energy photoelectrons emitted from He atoms by means of very narrow band synchrotron radiation. In a COLTRIMS setup two position and time sensitive detectors are used to measure the momenta of ions and electrons in coincidence. A weak electric field guides the electron and the ions to their respective detectors. It is the effect of this weak extraction field on the photoionization process, which is under investigation in this article. In more detail, the spectrometer consisted of a region with a uniform electric field and on the

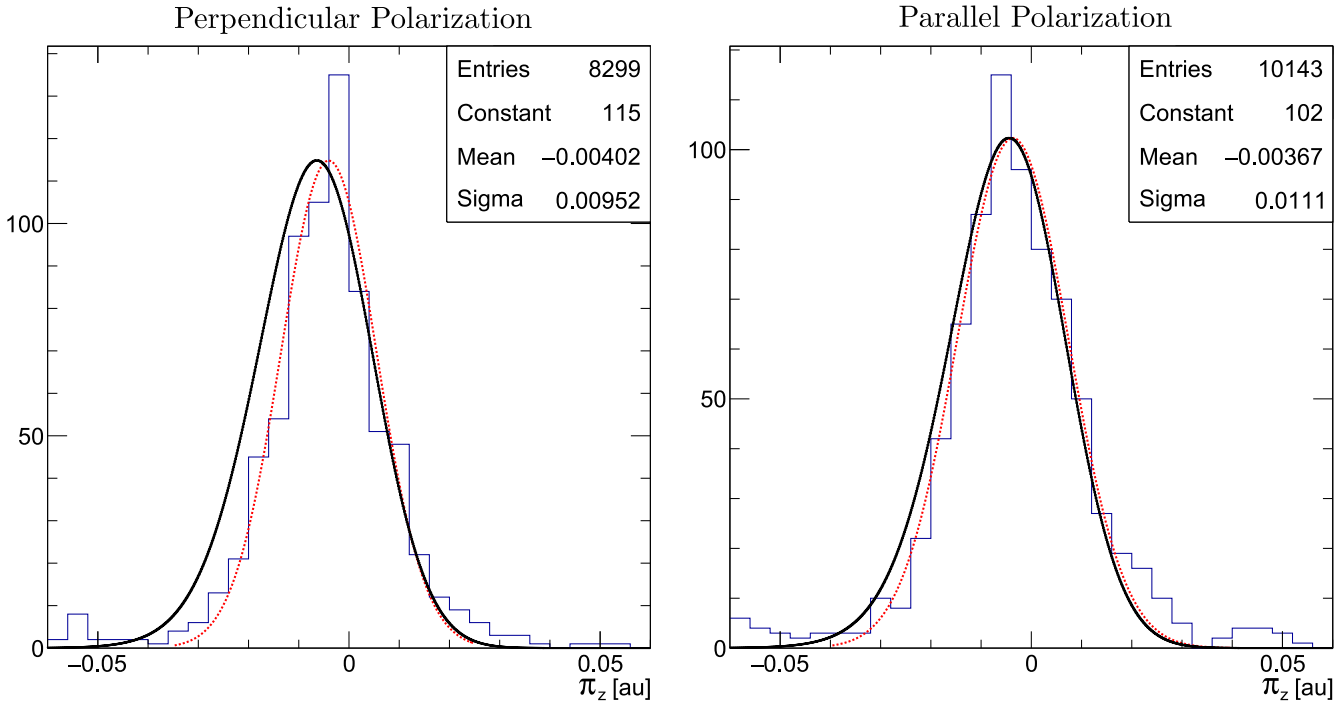


**Figure 5.** Direct comparisons of the experiment and theory for a 10 V cm$^{-1}$ extraction field. Red dashed curves show a Gaussian fit to the experimental data. Black curves are the theoretical calculations.

electron arm of the spectrometer a Mclaren-time-focusing approach was implemented (7 cm of acceleration followed by 14 cm of a field-free drift region) compensating for the width of the supersonic jet in the $z$-direction (i.e. along the spectrometer axis). Three different electric field settings were used to in the experiment: 1 V cm$^{-1}$, 10 V cm$^{-1}$, 40 V cm$^{-1}$. Electrons were collected with $4\pi$ solid angle for all three electric field settings, since the electrons have only very little initial momentum.

The experiment was performed at beamline UE112_PGM-1 of the Berlin Electron Storage Ring Society for Synchrotron Radiation (BESSY) using both vertically and horizontally polarized light. The photon energy was scanned between 24.581 and 24.593 eV along with two runs at fixed energies of 24.609 and 24.585 eV. The photons from the synchrotron intersected the supersonic helium gas jet, which in turn produced either excited Rydberg type states or singly ionized helium atoms depending on the photon energy. For photon energies between the field free ionization threshold and the field modified barrier a fraction of the excited electrons escapes while the rest remains trapped. The escape fraction depends on the strength of the extraction field and the relative direction between the light's polarization and the extraction field.

The calibration of the photon energy $\hbar\omega$ relative to the field-free threshold was critical to understand the result of this experiment and was achieved via the abundance curve. When the polarization vector is parallel to the electric extraction field the abundance is given by the following equation, cf discussion around equation (5) for the derivation,

$$S_{\parallel}(E) = \begin{cases} 1 & \text{for } 0 < E, \\ 1 - \frac{3}{4}E^2/F + \frac{3}{8}E^4/F^2 - \frac{1}{16}E^6/F^3 & \text{for } E_b \leqslant E \leqslant 0 \\ 0 & \text{for } E < E_b. \end{cases} \tag{8}$$

We reiterate here, that the barrier top $E_b$ depends on the strength of the extraction field and is given by $E_b = -2\sqrt{F}$. The abundance curve (8) is shown in figure 1 for the case where a 10 V cm$^{-1}$ extraction field was utilized.

The true position of the field-free zero point was found by examining and comparing the experimental and theoretical abundance. As the photon resolution was determined to be approximately 1.7 meV, the theoretical abundance equation was convoluted with this resolution to better match the experimental data. By examining the energy position of 50% abundance in the convoluted theory curve, we were able to determine the field-free threshold for the experimental data.

## 4. Results

The results presented here show a clear shift in the measured apparent momentum of the electron which is also verified by theoretical calculations. We produced several different photon energy scans each with a different electric extraction field. This allows us to compare and contrast the effect that the different field strengths have on the electron's momentum. Additionally, we separately measured several longer fixed

energy datasets at 10 V cm$^{-1}$ that allow us to more accurately determine the exact shift.

The observed apparent negative average momentum shift is due to the fact that an emerging electron is slowed down above the potential barrier. Thus the corresponding time of flight $t_{of}$ increases rendering the apparent effective momentum $\pi$, cf equation (7), more negative. This retarded motion occurs most notably for energies just above the top of the barrier, say $E_b < E \lesssim 0$. Well above the barrier (say $E > 0$) this effect becomes less important, the average effective momentum becomes $\langle \pi_z \rangle = 0$.

### 4.1. 1 V cm$^{-1}$

Firstly, we examine the effect an 1 V cm$^{-1}$ extraction field as shown in figure 2. There we show the abundance of electrons versus the photon energy (relative to the field-free ionization threshold) and the effective momentum in the $z$-direction. We also show the mean momentum, which is determined with a Gaussian fit, versus the photon energy. Furthermore, cases for both orientations of the polarization—parallel to the electric field and perpendicular to the electric field—are examined. The theoretical results shown in figures 2–4 have been blurred with experimental momentum resolution. At this extraction field the apparent momentum shift is very small and appears to be within our experimental resolution (shown as horizontal black lines in figure 2).

### 4.2. 10 V cm$^{-1}$

In figure 3 we again have the same type of plots as we did in figure 2. When we increase the extraction field to 10 V cm$^{-1}$ there is a markedly more visible effect, though this is in part due to the considerably better statistics that we have in these two particular scans. The maximum effect in the perpendicular orientation is a $-0.0053 \pm 0.0005$ a.u. shift in the momentum at $-1.9$ meV. Whereas the parallel orientation is shifted by $-0.0053 \pm 0.0009$ a.u. in momentum at $-2.1$ meV. The light blue ghost image at around $-0.07$ a.u. is an experimental artifact caused by our electron detector.

### 4.3. 40 V cm$^{-1}$

When we increase the extraction field to 40 V cm$^{-1}$ we can see that the momentum resolution in the $z$-direction is substantially reduced. Additionally, we are again hampered by poor statistics. But there is still a visible shift in the measured momentum distribution. The perpendicular orientation's maximum shift is $-0.010 \pm 0.0020$ a.u. in momentum at $-3.3$ meV. Whereas the parallel orientation is shifted by $-0.0073 \pm 0.0021$ a.u. in the momentum at $-3.9$ meV. Both orientation roughly match their respective theory plot. Additionally, there is even a slight deviation visible in the experimental data plot for parallel polarization at about $-1$ meV, which matches the prediction.

### 4.4. Fixed energies 10 V cm$^{-1}$

In an effort to improve the experimental results additional data was taken at a single fixed energy for the 10 V/cm extraction field. This is shown for both polarizations in figure 5. Unfortunately, a photon energy of 24.585 eV was chosen, which turns out be at $E_b$. Since this photon energy is at the barrier it will lead to distorted results, because the photons have a resolution of about 1.7 meV. Therefore, roughly half of the photon distribution is excluded from producing photoelectrons and only the part above the barrier will be useful for us. This produces an effective shift in the median photon energy. When theory compensates for this difficulty we see relatively good agreement.

## 5. Conclusion

We see the predicted trend in the data that an increasing extraction field strength causes an increasingly negative effective momentum. While this effect is small, and thus could possibly be ignored in some experiments, it has to be treated carefully. Electron spectroscopy usually builds on the assumption that at least conceptually the measurement apparatus and the atomic process which creates the investigated electrons can be separated. One assumes that the ionization process sets electrons free with a well-defined momentum vector. This momentum vector is then converted by the electron spectrometer into a quantity which is experimentally accessible (e.g. time-of-flight, position on a detector, or a trajectory in an analyzer). It is this separation of the atomic process and the spectrometer which fails in the situation at the ionization threshold discussed in this paper. While in general an influence of an electric field on the atomic effects is known, the tiny field magnitude at which this effect becomes observable in spectroscopy is remarkable.

## Acknowledgments

We would like to thank BESSY II and beamline UE112_PGM-1 for their excellent help with this experiment. The work was supported by DFG and BMBF.

## References

[1] Hogan P B, Smith S J, Georges A T and Lambropoulos P 1978 *Phys. Rev. Lett.* **41** 229
[2] Luc-Koenig E and Bachelier A 1979 *Phys. Rev. Lett.* **43** 921
[3] Tajima T and Dawson J M 1979 *Phys. Rev. Lett.* **43** 267
[4] Nicole C, Sluimer I, Rosca-Pruna F, Warntjes M, Vrakking M, Bordas C, Texier F and Robicheaux F 2000 *Phys. Rev. Lett.* **85** 4024
[5] Lankhuijzen G M and Noordam L D 1996 *Phys. Rev. Lett.* **76** 1784

[6] Held A and Schlag E W 1998 *Acc. Chem. Res.* **31** 467–73
[7] Yan T M, Popruzhenko S V, Vrakking M J J and Bauer D 2010 *Phys. Rev. Lett.* **105** 1079–7114
[8] Blaga C I, Catoire F, Colosimo P, Paulus G G, Muller H G, Agostini P and DiMauro L F 2009 *Nat. Phys.* **5** 335–8
[9] Quan W *et al* 2009 *Phys. Rev. Lett.* **103** 1079–7114
[10] Kästner A, Saalmann U and Rost J M 2012 *Phys. Rev. Lett.* **108** 1079–7114
[11] Kästner A, Saalmann U and Rost J M 2012 *J. Phys. B: At. Mol. Opt. Phys.* **45** 074011
[12] Wu C Y, Yang Y D, Liu Y Q, Gong Q H, Wu M, Liu X, Hao X L, Li W D, He X T and Chen J 2012 *Phys. Rev. Lett.* **109** 1079–7114
[13] Guo L *et al* 2013 *Phys. Rev. Lett.* **110** 1079–7114
[14] Becker W, Goreslavski S P, MiloševićD B and Paulus G G 2014 *J. Phys. B: At. Mol. Opt. Phys.* **47** 204022
[15] Möller M, Meyer F, Sayler A M, Paulus G G, Kling M F, Schmidt B E, Becker W and Milošević D B 2014 *Phys. Rev. A* **90** 1094–622
[16] Zhang K *et al* 2016 *Phys. Rev.* A **93** 021403(R)
[17] Diesen E, Saalmann U, Richter M, Kunitski M, Dörner R and Rost J M 2016 *Phys. Rev. Lett.* **116** 1079–7114
[18] Lantoine G and Russell R P 2011 *Celest. Mech. Dyn. Astron.* **109** 333
[19] Dörner R, Mergel V, Jagutzki O, Spielberger L, Ullrich J, Moshammer R and Schmidt-Böcking H 2000 *Phys. Rep.* **330** 95–192
[20] Ullrich J, Moshammer R, Dorn A, Dörner R, Schmidt L P H and Schmidt-Böcking H 2003 *Rep. Prog. Phys.* **66** 1463
[21] Jahnke T, Weber T, Osipov T, Landers A, Jagutzki O, Schmidt L, Cocke C, Prior M, Schmidt-Böcking H and Dörner R 2004 *J. Electron Spectrosc. Relat. Phenom.* **141** 229–38